Radiolysis of Liquid Water at Temperatures up to 300 °C: A Monte Carlo Simulation Study

Marie-Anne Hervé du Penhoat, Thomas Goulet, Yvon Frongillo, Marie-Josée Fraser, Philippe Bernat, and Jean-Paul Jay-Gerin*

Département de Médecine Nucléaire et de Radiobiologie, Faculté de Médecine, Université de Sherbrooke, Sherbrooke (Québec) J1H 5N4, Canada

Received: May 3, 2000; In Final Form: August 17, 2000

Monte Carlo simulations were performed to calculate the temperature dependence of the primary yields (*g*-values) of the radical and molecular products of the radiolysis of pure, deaerated liquid water by low linear-energy-transfer (LET) radiation. The early energy deposition was approximated by considering short segments (∼100 μm) of 300-MeV proton tracks (corresponding to an average LET of ∼0.3 keV/μm). The subsequent nonhomogeneous chemical evolution of the reactive species formed in these tracks was simulated by using the independent reaction times approximation, which has previously been used successfully to model the radiolysis of liquid water at ambient temperature under various conditions. Our calculated *g*-values for the radiolytic species: e_{aq}^-, OH, H, H_2, and H_2O_2, are presented as a function of temperature over the range 25−300 °C. They show an increase in $g(e_{aq}^-)$, g(OH), and [g(H) + $g(H_2)$] and a decrease in $g(H_2O_2)$ with increasing temperature, in agreement with existing experimental data. The sensitivity of the results to the values of reaction rate constants and to the temperature dependence of electron thermalization distances (r_{th}) was also investigated. It was found that the best agreement with experiment occurs when the distances of electron thermalization decrease with increasing temperature, a result that is at variance with the predictions of previous modeling studies. Such a decrease in r_{th} as the temperature increases could be linked to an increase in the scattering cross sections of subexcitation electrons that would account for the corresponding decrease in the degree of structural order of water molecules. Our simulations also suggest that the variations of the *g*-values with temperature, and especially that of $g(H_2)$, are better described if we account for the screening of the Coulomb forces between the two e_{aq}^- in the bimolecular self-reaction of the hydrated electron. Finally, the time-dependent yields of e_{aq}^- and OH are presented as functions of temperature, in the range 10^{-12}−10^{-6} s. It was found that the temporal variation of $g(e_{aq}^-)$ at elevated temperatures is sensitive to the temperature dependence of r_{th}, suggesting that measurements of the decay of hydrated electrons as functions of time and temperature could, in turn, provide information on the thermalization of subexcitation electrons. The good overall accord of our calculated results with the experimental data available from the literature demonstrates that Monte Carlo simulation methods offer a most promising avenue at present to further develop our understanding of temperature effects in the radiolysis of liquid water.

1. Introduction

A detailed knowledge of the γ-radiolysis of liquid water at elevated temperatures is an important factor in the overall chemistry occurring in water-cooled/moderated nuclear reactor systems, which operate with typical temperatures in the range ∼250−315 °C.[1−6] The key parameters are the "primary" yields or *g*-values (defined as a number of species per 100 eV of absorbed energy) of the radical and molecular products of water radiolysis (e_{aq}^-, H, OH, H_2, H_2O_2, H_3O^+...) and the rate constants and activation energies of their interreactions. These products are associated with deleterious corrosion and hydriding processes in the core and in the various piping components of the reactors.[1,5,7]

Understanding these processes involves knowledge of the early energy deposition and the subsequent physicochemical and nonhomogeneous chemical evolution of the system to times, at room temperature, on the order of 10^{-6} s, after which the remaining radiolytic products are usually regarded as homogeneously distributed in the bulk of the solution.[8,9] Such a short temporal domain is not easily accessible experimentally, especially since we wish to study the effects of high temperature on water radiolysis. In this work, we have extended our recently developed Monte Carlo simulation studies of the radiolysis of liquid water[10,11] to account precisely for processes over the temperature range from ambient up to 300 °C. Using these simulations, the *g*-values of all the radiolytic species are calculated as functions of time and temperature for low linear-energy-transfer (LET) radiation corresponding essentially to ^{60}-Co γ-rays (mean photon energy 1250 keV) or X-rays of the same energy. The results of the calculations are compared with the available experimental data and other theoretical models. In addition, a detailed study of the sensitivity of the results to the values of reaction rate constants and to the temperature dependence of electron thermalization distances has also been performed in an effort to estimate the impact of those factors on the calculated yields.

* Corresponding author. Tel.: 1-819-346-1110, ext. 14682. Fax: 1-819-564-5442. E-mail: jaygerin@courrier.usherb.ca.

10.1021/jp001662d CCC: $19.00
Published on Web 11/28/2000

A preliminary report of this work has been presented elsewhere.[12]

2. Method and Reaction Scheme

It is usual to divide into three main temporal stages the series of events that take place in liquid water following the absorption of ionizing radiation. Here, we briefly describe those stages and the approach used to model them through stochastic simulation methods. Since a detailed description of the principles of our simulation methodology has already been published,[10,11] we will restrict this presentation to the most essential features. In view of the focus of the present paper, we will outline the influence of the temperature on the unfolding of each stage.

The first stage—called the "physical stage"—consists of the period prior to 10^{-14} s, during which energy is deposited by the primary radiation particles and by all of the secondary (tertiary, and so forth) electrons that result from the ionization of the water molecules. This energy deposition occurs through the slowing down of those particles via a variety of inelastic scattering processes, including ionization, electronic and/or vibrational excitation of single water molecules, and excitation of plasmon-type collective modes. The simulation codes that we use to cover this stage are TRACPRO and TRACELE, which describe the detailed transport and slowing down of incident protons and electrons, respectively.[10] To reproduce the effects of ^{60}Co γ-radiolysis, we use short track segments ($\sim$100 μm) of 300-MeV protons over which the average LET value obtained in the simulations is $\sim$0.3 keV/μm.[6] As has already been shown,[11] these protons, through appropriate choices of their initial energies, act as excellent model particles for various LET radiation types.

All the events of the physical stage are simulated by a "step-by-step" method that describes each scattering event, recording the position of the energy deposition, the actual amount of energy lost by the scattered particle, its angular deflection, and modification caused locally to the medium. If a secondary electron is produced through ionization, its initial physical parameters (starting point, energy, and direction of motion) are also recorded for further processing of its transport and action in the medium. The stochastic selection of the scattering events is done with various sampling techniques (direct inversion, etc.) in accordance with the appropriate scattering cross sections for each process.[10]

The scattering cross sections used in the simulations are independent of the medium's temperature because the energy of the ionizing particles is much larger than the thermal energies and because the motion of the target (water) molecules can be neglected. However, the density (ρ) of pressurized water varies with temperature (from $\rho = 1$ g/cm^3 at room temperature to $\rho = 0.7125$ g/cm^3 at 300 °C),[1] and this influences the particle's scattering mean free paths (MFP) which are related to the scattering cross sections through the simple relation MFP $= 1/(\sigma N)$, where σ is the total cross section and N is the number of scatterers per unit volume. The $\sim$30% decrease in N that takes place when the temperature is increased from 25 to 300 °C thus causes the energy depositions to become significantly further apart. As a result of the invariance of the scattering cross sections, this dilatation is proportional to the inverse of the density. Physically, this means that temperature brings the water molecules further apart but does not change their ability to interact with the energetic particles.

The second stage—called the "physicochemical stage"—consists of the period during which the energy that has been deposited in the medium is used to produce the initial chemical species of the radiolysis. This intermediate stage between the purely physical (energy deposition) and purely chemical events of water radiolysis is handled by our simulation code TRACELE.[10] During this period, which extends from $\sim 10^{-14}$ to 10^{-12} s, there is not time enough for appreciable diffusion to take place. The electronically excited water molecules (H_2O^*) undergo transformations that can lead to their autoionization, dissociation, or simply a return to the ground state. The ionized water molecules (H_2O^+) are allowed to migrate via a sequence of electron transfers to the H_2O^+ hole before a proton-transfer reaction occurs. This latter reaction with a neighboring water molecule leads to the formation of OH radicals and H^+ (H_3O^+) ions. As for the "subexcitation electrons",[13] they relax through a series of vibrational and rotational excitations of the water molecules[14] and, in doing so, migrate to a point where they are thermalized, then trapped between water molecules, and finally hydrated (e^-_{aq}). The distance that separates the initial position of the subexcitation electron and the position at which it becomes hydrated is herein referred to as the "electron thermalization distance" r_{th}, on the basis of the conjecture that electron thermalization, trapping, and hydration follow in quick succession.[15] In the simulations, electron thermalization is modeled by a random walk that gives rise to a distribution of r_{th} values.[16,17] One should note that in the course of its thermalization, the subexcitation electron can encounter an H_2O^+ ion and recombine to form H_2O^*.[15] It can also form a transient anion H_2O^-, which quickly undergoes dissociation with the release of H^- and OH, the hydride ion then reacting immediately with another water molecule via a proton transfer to give H_2 and OH^-.[18]

The influence of the temperature on the physicochemical stage is not well understood. On one hand, the possible decay channels for H_2O^+ and H_2O^* are likely to be essentially independent of temperature since those primary processes are not thermally activated. This assumption of temperature independence has been adopted in the present work. It should be mentioned, however, that other authors, such as Swiatla-Wojcik and Buxton[19] (hereafter referred to as SWB), have suggested that the temperature—through a diminution of hydrogen bonding in liquid water—could possibly change the relative contributions of the dissociative decay channels for H_2O^* (see section 3.1.5). On the other hand, the migration of the ions H_2O^+ and of the subexcitation electrons is likely to be sensitive to temperature. First of all, the variations of density would act as they did in the physical stage, increasing (on average) each step of the random walk. But any number of other phenomena could come into play. For example, when a "hot" (subvibrational) electron is slowing down before eventually getting trapped, it goes through a stage during which its energy is nearly thermal, so that it cannot only lose energy but also gain some from the surrounding medium. If the duration of this quasi-equilibrium stage depends on temperature, it could affect the electron thermalization distances.

Another temperature effect, that could turn out to be the most important one in the physicochemical stage, is its influence on the scattering cross sections of the low-energy electrons. In fact, electrons in the subexcitation energy range are known to be sensitive to the structural order of the surrounding medium, owing to their nonnegligible delocalized character. In various media, their scattering cross-sections have been shown to increase rapidly when the degree of order diminishes.[20] This also seems to be the case for water, since the electron cross sections found in amorphous ice at low incident energy[21] appear to be somewhat smaller (by a factor of $\sim$2) than those that apply

to liquid water[10,17] and much smaller (by at least an order of magnitude) than those reported for the gas phase.[21] On this basis, one could expect the scattering cross sections of subexcitation electrons to increase with temperature in the range 25−300 °C, since the breaking of the hydrogen bonds gives rise to a decrease of the structural order. It is difficult to estimate to what extent this could affect thermalization distances, but one cannot exclude the possibility that this effect could overcome the ∼30% decrease in the density as temperature increases from 25 to 300 °C and in turn reduce those distances significantly. A similar conclusion was obtained previously by Hochanadel and Ghormley,[22] who suggested that, at higher temperature, "subexcitation electrons are thermalized more rapidly". We will show in section 3.3 that, indeed, our simulations better reproduce the experimental yields if electron thermalization distances decrease with increasing temperature.

It should be noted that the temperature effects that we mentioned do not modify the initial yields of the radiolytic species. In contrast, they can significantly affect the initial spatial distribution of those species and, in turn, their subsequent reaction kinetics.

The third and final stage that we consider here—called the "stage of nonhomogeneous chemistry"—consists of the period after $\sim 10^{-12}$ s, during which the radiolytic species diffuse and react with one another with a kinetics dictated by their initial nonhomogeneous spatial distribution. At room temperature, this stage is essentially completed on the microsecond time scale,[11,23] after which homogeneous chemistry takes over. To model the chemical development occurring during this stage, we use a simulation approach called the "independent reaction times" (IRT) method,[24] which considers all the possible pairs of reactants created in the entire particle track and stochastically samples the order in which the competing reactions will occur. The sorting of the sampled reaction times allows the discarding of events that would involve species that have already reacted. The code that we use to perform this simulation is called TRACIRT. Its implementation has been described in detail,[11] and its validity has been established through a comparison with a full step-by-step Monte Carlo simulation method.[25] This code has already been used to model the radiolysis of liquid water at ambient temperature for radiation tracks of various LET, ranging from ∼0.3 to 20 keV/μm.[11]

The stage of nonhomogeneous chemistry is certainly the period during which the temperature is playing its most prominent role on the radiolytic process. Our description of this stage as a function of temperature differs from those of SWB[19] and of LaVerne and Pimblott[26] (hereafter referred to as LP) in many respects. The most important difference is that, contrary to these authors, who describe a concentration gradient of reactants, we take into account in this work the stochastic nature of the reactions, since we follow the radiolytic species one by one. Moreover, we do not have to use idealized *average spurs*, which are inaccurate, since they fail to account for the wide variety of clusters of species that can be found along the radiation tracks. In fact, we can directly use the complex spatial distribution of reactants at $\sim 10^{-12}$ s that is provided as an output of the program TRACELE.[10] We thus benefit here from having developed a full Monte Carlo simulation code that integrates the three temporal stages of water radiolysis listed above.

Some chemical reactions can take place before any diffusion of the species occurs because they are already in contact at the end of the physicochemical stage.[10,11] For simplicity, we consider that those "contact reactions" occur at $\sim 10^{-12}$ s, that is, at the starting point of the nonhomogeneous kinetics. The occurrence of all the other reactions depends on the ability of reactants to meet and on the probability that their encounter gives rise to a reaction (most reactions are not diffusion-controlled). The physical parameters that will determine the time-dependent reaction probability of a pair of reactants will therefore be (i) their initial separation, (ii) their diffusion coefficient, (iii) their electrostatic interaction (i.e., their charge and the dielectric constant of the medium), (iv) their reaction radius, and (v) their probability of reaction per encounter. The temperature of the medium has an influence on many of those parameters. We examine successively these effects below.

TABLE 1: Values at 25 °C for the Diffusion Coefficients (D_I) and Reaction Radii (r_I) of the 15 Reactive Species (I) Involved in Our Simulations (See refs 11 and 27)[a]

species (I)	D_I (25 °C) (10^{-9} m^2 s^{-1})	temperature dependence adopted for D_I	r_I (25 °C) (nm)
e_{aq}^-	4.9	tabular (ref 27) (t < 90 °C)	0.5
		Arrhenius relationship (t > 90 °C)	
H^+	9.46	tabular (ref 27)	0.25
H	7.0	self-diffusion of water	0.19
OH	2.2	self-diffusion of water	0.22
H_2O_2	2.3	self-diffusion of water	0.21
H_2	4.8	self-diffusion of water	0.14
OH^-	5.3	tabular (ref 27)	0.33
O_2	2.4	self-diffusion of water	0.17
O_2^-	1.75	self-diffusion of water	0.22
HO_2	2.3	self-diffusion of water	0.21
HO_2^-	1.4	self-diffusion of water	0.25
$O(^3P)$	2.0	self-diffusion of water	0.2
O^-	2.0	self-diffusion of water	0.25
O_3^-	2.0	self-diffusion of water	0.2
O_3	2.0	self-diffusion of water	0.2

[a] The temperature dependence adopted for D_I is given for each reactant. The polynomial for describing the self-diffusion of water (D_{H_2O}) between 0 and 300 °C is taken from ref 27. Note that D_{H_2O} does not follow an exact Arrhenius dependence; the apparent activation energy over 0−300 °C is ∼15.5 kJ/mol (ref 27). H^+ is used as an abbreviation for the hydronium ion H_3O^+ and $O(^3P)$ corresponds to the oxygen atom in its ^3P ground state.

The effect of temperature on the initial position of the species comes from the temperature dependence of the scattering mean free paths mentioned in the first two stages. Its influence on the diffusion coefficient depends on the actual species considered, but this parameter always increases with temperature. In the simulation, the temperature dependences for the diffusion coefficients of H_3O^+ and OH^- are represented by polynomial fits to the experimental data, as reported by Elliot.[27] Such a polynomial representation is also used for the diffusion coefficient of e_{aq}^- over the 4−90 °C temperature range. Above 90 °C, this coefficient is represented by an Arrhenius expression with an activation energy of 20.75 kJ/mol.[27] For the other species, whose diffusion coefficients are unknown at elevated temperatures, the following scaling procedure has been adopted:

$$D_I(t) = D_I(25\ °C)\,\frac{D_{H_2O}(t)}{D_{H_2O}(25\ °C)} \qquad (1)$$

where t denotes the temperature in degrees Celsius. In this procedure, the temperature dependence for diffusion of a given reactant (I) is assumed to be the same as that for the self-diffusion of water (D_{H_2O}).[27,28] The diffusion coefficients (D_I) at 25 °C used in the calculations are listed in Table 1. The polynomial expression for the temperature dependence of D_{H_2O} up to 300 °C is taken from Elliot.[27] As shown by this author,[27] self-diffusion in water does not follow an exact Arrhenius dependence; the apparent activation energy over the 0−300 °C

range is ~15.5 kJ/mol. The fitting procedures for the diffusion coefficients of the various species involved in the radiolysis of water are summarized in Table 1.

The importance of Coulomb forces can be accounted for through the variation of the Onsager radius (r_c),[29] which represents some sort of range of the Coulomb field. Formally, r_c is the distance at which the Coulomb potential energy between two singly charged ions is equal in magnitude to k_BT, where k_B is Boltzmann's constant and $T = t + 273.15$ is the absolute temperature of the medium in Kelvin (for water, $r_c \approx 0.715$ nm at 25 °C if we use a dielectric constant $\epsilon = 78.4$).[30] On this basis, one could think that increasing the thermal energy would reduce the role played by the Coulomb forces, but it is exactly the opposite phenomenon that takes place. This is because an increase in temperature brings disorder in the molecular dipoles constituent of the medium and, in turn, reduces its dielectric constant (for water, ϵ goes from ~78.4 at 25 °C to ~19.7 at 300 °C).[30]

The influence of the temperature on the reaction radii of the reacting species and on the probability of reaction in a given encounter (P_{react}) is a rather complex matter. What is generally known is the temperature dependence of the observed reaction rate constant (k_{obs}), from which it is possible to extract information on the temperature dependences of the activation and diffusion processes that are involved in the reaction.[27] Indeed, a valuable method for a mathematical representation of the measured rate constant for a reaction is based on the Noyes equation:[31]

$$\frac{1}{k_{obs}} = \frac{1}{k_{diff}} + \frac{1}{k_{act}} \tag{2}$$

where the reciprocal of the measured value is represented by the sum of the reciprocals of the diffusion and activation components of k_{obs}. k_{diff} is given by the Smoluchowski equation:[32]

$$k_{diff}(T) = 4\pi\beta N_{Av}\, D(T)\, r \tag{3}$$

where N_{Av} is Avogadro's number, D is the sum of diffusion coefficients for both reacting species, β is the spin statistical factor for radical−radical reactions, and r is the reaction distance (i.e., the sum of the reactant reaction radii). Note that, in the case of a reaction between particles of the same species, the term 4π becomes 2π in order to avoid counting twice every pair of reactants. When the reactants (A and B, for instance) are both ions, eq 3 can be generalized with the help of the Debye factor $f_D = \delta/(e^\delta - 1)$, and k_{diff} is given by the Debye equation:[33]

$$k_{diff}(T) = 4\pi\beta N_{Av}\, D(T)\, r\, f_D(T) \tag{4}$$

where

$$\delta = \frac{Z_A Z_B e^2}{4\pi\epsilon_0\epsilon(T) r k_B T} \tag{5}$$

Z_A and Z_B are the charges on the ions, e is the electron charge, ϵ_0 is the permittivity of vacuum, and $\epsilon(T)$ is the dielectric constant of the medium.

In our simulations, the reactions between the species A and B are divided into six types (1−6).[11] Depending on the data available and on the reaction type, r and P_{react} were extracted by different methods. The values at 25 °C for the reaction radii (r_I) of the various intervening species (I) are listed in Table 1. In general, $r = r_A + r_B$ is assumed not to change with temperature. Reactions of types 1 and 3 are fully diffusion controlled, so that $P_{react} = 1$ and k_{obs} is equal to k_{diff}. As a result of this, experimental data for k_{obs} can be modeled by eq 3 or 4. This fitting procedure is referred to as DC in Table 2. It should be noted that, for certain type 1 or 3 reactions (referred to as DC* in Table 2), the experimental data for k_{obs} (= k_{diff}) are fitted to an Arrhenius equation, so that in those particular cases, r is no longer equal to the sum of the reactant reaction radii, though it remains independent of temperature. The difference between reactions of types 1 and 3 lies in the fact that, in the former, Coulomb interactions between the reactants do not intervene, while they are involved in the latter (reactions between charged species).[11] Reactions of types 2 and 4 correspond to reactions that are partially diffusion-controlled ($P_{react} < 1$), and P_{react} is given by[34]

$$P_{react} = \frac{\exp\left(-\frac{r_c}{r}\right) - \exp\left(-\frac{r_c}{r+\chi}\right)}{\left[\exp\left(-\frac{r_c}{r}\right) - \exp\left(-\frac{r_c}{r+\chi}\right)\right] - \frac{k_{diff}}{k_{act}}\left[1 - \exp\left(-\frac{r_c}{r}\right)\right]} \tag{6}$$

where χ is the distance that separates the reactants after an unreactive encounter (taken here as 0.3 nm). Hence, extracting k_{act} from the experimental data for k_{obs} enables us to determine P_{react}. Note that eq 6 is equally valid for the cases where Coulomb interactions are not involved (type 2 reactions) or intervene (type 4 reactions).[11] For reactions whose rates are not influenced by diffusion, the experimental data for k_{obs} are fitted to an Arrhenius relationship. k_{act} is deduced at each temperature

TABLE 2: Main Reaction Scheme Inferred from Our Monte Carlo Simulations of the Radiolysis of Pure, Deaerated Liquid Water at Temperatures in the Range 25−300 °C[a]

symbol[b]	reaction	type	A_0	E_A	fit
R1	$e_{aq}^- + OH \rightarrow OH^-$	2	0.0304	−3.5	N
R2	$e_{aq}^- + H^+ \rightarrow H$	4, 6	1.24	10.1	A
	$H \rightarrow e_{aq}^- + H^+$	6	−	−	PO1
R3	$e_{aq}^- + e_{aq}^- \rightarrow H_2 + 2OH^-$	5	−	−	DC
R4	$e_{aq}^- + H \rightarrow H_2 + OH^-$	5	7.52	14.0	A*
R5	$e_{aq}^- + H_2O_2 \rightarrow OH + OH^-$	2	6.26	14.0	N
R6	$e_{aq}^- + H_2O \rightarrow H + OH^-$	6	−	−	RW
	$H + OH^- \rightarrow e_{aq}^- + H_2O$	2, 6	133	38.8	A
R7	$OH + OH \rightarrow H_2O_2$	2	0.0369	3.0	N
R8	$H + OH \rightarrow H_2O$	2	0.178	4.5	N
R9	$OH + OH^- \rightarrow O^- + H_2O$	2, 6	−	−	P
	$O^- + H_2O \rightarrow OH + OH^-$	6	−	−	RW
R10	$H + H \rightarrow H_2$	5	−	−	DC
R11	$H^+ + HO_2^- \rightarrow H_2O_2$	4, 6	−	−	P
R12	$H^+ + OH^- \rightarrow H_2O$	3, 6	−	−	DC
R13	$H^+ + O^- \rightarrow OH$	4, 6	−	−	P
R14	$H + O(^3P) \rightarrow OH$	1	10.9	15.6	DC*

[a] For a description of the full reaction scheme considered in our simulations, see ref 11. The temperature dependences of the rate constants were obtained from ref 27 (see also ref 11). The classifications of the reaction types (1−6) and of the fitting procedures [DC, DC*, A, A*, P, N, PO1, and RW] are explained in the text. Briefly, DC refers to k_{obs} being fitted by a Smoluchowski or Debye equation (eq 3 or 4); DC*, A, and A* correspond to Arrhenius fits to k_{obs}; P refers to a polynomial fit to k_{obs}; N corresponds to an Arrhenius fit to k_{act}; PO1 are pseudo-first-order reactions; and RW refers to reaction rate constants determined with equilibrium equations. A_0 (preexponential factor, in 10^{12} M^{-1} s^{-1}) and E_A (activation energy, in kJ/mol) are the parameters of the Arrhenius equation. The Arrhenius expression is given by $k = A_0 \exp(-E_A/RT)$, where R is the molar gas constant and $RT = 2.479$ kJ/mol at 25 °C. H^+ is used as an abbreviation for the hydronium ion H_3O^+. [b] Reaction symbols used in the text.

from eq 2. This fitting procedure is referred to as A in Table 2. For the other reactions of types 2 and 4, various fitting procedures have been used. In some cases (referred to as P in Table 2), the data for k_{obs} are fitted to a polynomial expression taken from Elliot[27] and k_{act} is deduced from eq 2. In other cases, referred to as N in Table 2, k_{act} is fitted to an Arrhenius equation so that k_{obs} best reproduces the experimental data when calculated from eq 2.

Reactions of type 5 correspond to the case where a spin statistical factor affects the calculated diffusion-controlled reaction rate constant (because, for two radicals, only the singlet configuration of their combined spins allows the occurrence of the reaction—in contrast to the unreactive triplet configuration). In this case, $\beta = 0.25$ (i.e., one encounter in four can lead to a reaction). In our simulations, the persistence of the spin correlations is accounted for by setting $P_{react} = 0$ for each pair of reactants that has undergone an unreactive encounter and remains in a triplet state.[11] The inclusion of those spin effects is limited in this study to the reactions R3, R4, and R10 listed in Table 2.[11] The fitting procedures are the same as those for reactions of types 1 and 3, except for reaction R4 (referred to as A* in Table 2) for which the experimental data for k_{obs} ($= k_{diff}$) are fitted to an Arrhenius relationship,[27] so that in that case, r varies as a function of temperature.

As for reactions of type 6, they correspond to the first-order decay of a species or to pseudo-first-order reactions (referred to as PO1 in Table 2), which do not involve the encounter of two nonhomogeneously distributed reactants. In that case, the reaction times are sampled from an exponential function for which the characteristic decay time is the inverse of the homogeneous reaction rate constant.[11] Finally, in the case of equilibrium reactions (referred to as RW in Table 2), the reverse reaction is deduced as described by Elliot.[27]

Among the 54 reactions that are included in our simulations, only 14 reactions are needed to satisfactorily describe the nonhomogeneous chemical stage of liquid water radiolysis (see Table 2). It is found that other reactions involved in this radiolysis do not contribute to more than 1−2% to the primary yields of e^-_{aq}, OH, H, H_2O_2, and H_2 over the whole temperature range investigated. Fitting procedures and parameters for those reactions of the main reaction scheme are given in Table 2.

3. Results and Discussion

Systematic measurements of the g-values of radiolytic products in irradiated liquid water have recently been performed as a function of temperature by Elliot et al.[27,35] at the Chalk River Laboratories, Kent and Sims[36] at AEA Reactor Services, Harwell, and Ishigure and co-workers[37] at the University of Tokyo. The results of the temperature dependence of our g-values, computed at 10^{-7} s after the ionizing event, are compared with the observed yields in parts (a) and (b) of Figure 1 for the "reducing" (e^-_{aq}, H, and H_2) and "oxidizing" (OH and H_2O_2) species, respectively. Since the comparison of our computed yields was done mainly with the experimental data of Elliot et al.,[27,35] the time scale of 10^{-7} s is here chosen in accordance with the scavenging powers of solutes used by those authors to measure their g-values. This choice is also consistent with our Monte Carlo calculations, which show that the time at which the nonhomogeneous chemical stage is completed diminishes with increasing temperature, going from ~10^{-6} s at room temperature to about 10^{-7} s at 300 °C (see below and section 3.4). As we can see from Figure 1, there is good overall agreement between calculated and experimental values over the whole temperature range. Moreover, the criterion for a consistent

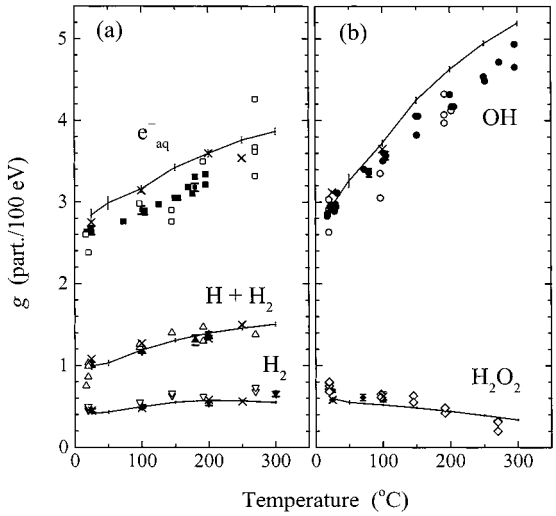

Figure 1. Variation of g-values (in part./100 eV) for the radiolysis of liquid water as a function of temperature: (a) "reducing" species $g(e^-_{aq})$, $[g(H) + g(H_2)]$, and $g(H_2)$ and (b) "oxidizing" species g(OH) and $g(H_2O_2)$. Simulated results, obtained at 10^{-7} s from averages over 150 track segments of 300-MeV protons (average LET ~ 0.3 keV/μm) (except at 25 and 50 °C where the simulated number of proton tracks is 40), are shown as a solid line. The error bars show the 95% confidence intervals of the simulation results. Experimental data are from refs 27 and 35 (closed symbols), ref 36 (open symbols), and ref 37 (crosses). The values for g(OH) from refs 27 and 35 were increased by 5% following normalization to a recent recalibration of the thiocyanate dosimeter (SCN^- in O_2-saturated water) system (ref 38) used to evaluate g(OH). It is also to be noted that, because of the large uncertainties in the g-values determined in ref 37 for both g(OH) and $g(H_2O_2)$ from the $HClO_4 + 10^{-2}$ mol kg^{-1} methanol chemical system at temperatures above 100 °C, these data are not shown in Figure 1b.

set of g-values (expressed in units of particles/100 eV[38]), given by the following balance equation:

$$g_{red} = g_{ox}$$

where

$$g_{red} = g(e^-_{aq}) + g(H) + 2g(H_2)$$

$$g_{ox} = g(OH) + 2g(H_2O_2) + 3g(HO_2) + g(O^-) + 2g(HO_2^-) + 3g(O_2^-) + 4g(O_2) + 2g[O(^3P)] + 5g(O_3^-) + 6g(O_3)$$

is satisfied by the results of our simulations: $|g_{red} - g_{ox}| < 0.001$.

Although Elliot et al.[27,35] estimated that their g-values were measured about 10^{-7} s following ionization, LP[26] and SWB[19] compared the experimental data to the results of their calculations at 10^{-6} s. Our results show that, although the yields of OH, H_2, and H_2O_2 remain nearly constant over the whole temperature range between ~10^{-7} and 10^{-6} s (within calculated uncertainty), the variations of $g(e^-_{aq})$ and g(H) in this time interval increase, in magnitude, with increasing temperature, from ~0.05 at 25 °C to ~1.5 at 300 °C (see section 3.4), mainly due to the reactions of e^-_{aq} with H^+ ions homogeneously distributed in the solution and with water:

$$e^-_{aq} + H^+ \rightleftarrows H \quad \Delta g(H)_{300\ °C} = 0.58 \text{ between } 10^{-7} \text{ and } 10^{-6} \text{ s}$$

$$e^-_{aq} + H_2O \rightleftarrows H + OH^- \quad \Delta g(H)_{300\ °C} = 0.94 \text{ between } 10^{-7} \text{ and } 10^{-6} \text{ s}$$

As a result, while the calculated values of $g(H)$ and $g(e_{aq}^-)$ at 10^{-7} s match all sets of experimental data as a function of temperature, their temperature dependences exhibit a completely different behavior at 10^{-6} s. Since those two pseudo-first-order reactions have not been taken into account in the spur model calculations of LP[26] and SWB,[19] the yields calculated by these authors show little change in the time range $10^{-7}-10^{-6}$ s and are therefore consistent with the experimental data.

The first and foremost observation that we can make from Figure 1 is that, with the exception of $g(H_2O_2)$, all yields increase with temperature. This general trend of having yields of reactants that increase with temperature can be attributed to the fact that many important reactions (such as, in particular, reactions R1 and R7 in the reaction scheme listed in Table 2) are not diffusion-controlled and therefore have rate constants that increase less steeply with temperature than do the diffusion coefficients of the reactive species.[39] One should note that, in the case of a diffusion-controlled reaction that does not involve Coulomb forces, the increase of the diffusion coefficient with temperature only affects the kinetics of the encounter of a pair of reactants and not their ultimate survival probability.[34] The decrease of $g(H_2O_2)$ with increasing temperature is also well explained by this general reasoning since hydrogen peroxide is primarily produced by the self-reaction of the hydroxyl radical (reaction R7). We could expect as well that the yield of a molecular product like H_2 would decrease with temperature. However, the case of H_2 is particular because it is mainly formed by reaction R3, which is diffusion-controlled. As will be discussed in sections 3.1.5 and 3.3, the quantitative description of the temperature dependence of $g(H_2)$ has drawn a great deal of attention and leads to many open questions.

As shown in Figure 1a, our calculated $g(e_{aq}^-)$ values exhibit a temperature dependence similar to that of the experimental data but are about 10% above in magnitude. As for the simulated OH radical yield (Figure 1b), it increases somewhat faster with temperature than the experimental values of Elliot et al.,[27,35] which were determined from the yields of CO_3^- radicals in the pulse radiolysis of aerated potassium hydrogencarbonate solutions. However, according to these authors,[35] it is possible that a temperature-dependent correction, based on the assumption of a temperature dependence of the molar absorption coefficient $\epsilon_{600\ nm}$ for CO_3^-, should be applied to part of their pulse radiolysis measurements. Such a correction would result in values for $g(OH)$ 7, 13, and 18% greater at 100, 200, and 300 °C, respectively, than the experimental results shown in Figure 1b.[35]

Below 150 °C, the experimental data for $g(H_2O_2)$ have a temperature dependence parallel to that of our simulated values but are 20% higher (Figure 1b). Above this temperature, the only available measurements of Kent and Sims[36] present a downward inflection, unlike the simulated curve. These latter authors[36] consider, however, that their measurements probably provide a lower limit for $g(H_2O_2)$. In addition, at elevated temperature, thermal decomposition of H_2O_2 may render experimental results unreliable.[36]

3.1. Contributions of the Various Reactions to the Radiolytic Yields. As already mentioned, the initial yields of the radiolytic species (before "contact reactions") are assumed in our simulations to be independent of the temperature. Hence, the variations of the yields of the various species with temperature only result from those reactions involved in their formation or decay. Computer simulation enables us to determine *quantitatively* the temperature dependence of each reaction. As mentioned above, the 14 reactions listed in Table 2 are those that contribute for more than 1−2% to the primary yields of e_{aq}^-, OH, H, H_2O_2, and H_2. Figures 2a−2e compare the effect of increasing temperature on the extent, expressed as a cumulative Δg-value, of each of the reactions of e_{aq}^-, OH, H, H_2O_2, and H_2 in the spurs as they expand by diffusion in the time interval $\sim 10^{-12}-10^{-7}$ s.

3.1.1. Production and Fate of Hydrated Electrons. Overall, the yield of e_{aq}^- increases linearly with temperature (Figure 1a). The three main reactions involved in the decay of e_{aq}^- are listed below in order of importance at 25 °C (note that this order is reversed above 150 °C; see Figure 2a):

$$e_{aq}^- + OH \rightarrow OH^-$$

$$\Delta g(e_{aq}^-) = -1.5 \text{ to } -0.2 \text{ from 25 to 300 °C} \quad \text{(R1)}$$

$$e_{aq}^- + H^+ \rightarrow H$$

$$\Delta g(e_{aq}^-) \approx -0.47 \text{ (nearly constant over all the temperature range)} \quad \text{(R2)}$$

$$e_{aq}^- + e_{aq}^- \rightarrow H_2 + 2OH^-$$

$$\Delta g(e_{aq}^-) = -0.24 \text{ to } -0.52 \text{ from 25 to 300 °C} \quad \text{(R3)}$$

One can see in Figure 2a that the contribution of reaction R1 to the decay of e_{aq}^- becomes less and less important as the temperature increases. This is due to the fact that the rate constant for this reaction increases much less steeply with temperature than the diffusion coefficient of the individual species.[41,42] As a consequence, more and more hydrated electrons are available as the temperature increases, to either react in other spur reactions (see the reaction scheme listed in Table 2) or escape into the bulk. The overall effect is that the contribution of the self-reaction R3, which is diffusion-controlled, is expected to increase at elevated temperatures (see section 3.1.5). As for reaction R2, however, its contribution is less predictable: on one hand, there are more hydrated electrons available but, on the other hand, the temperature dependence of the rate constant for this reaction is lower than that for the diffusion in water of the reactive species. Our simulation results show that those effects almost counterbalance one another, so that the contribution of reaction R2 can be regarded as being approximately independent of temperature over the range 25−300 °C. The deterministic diffusion−kinetic model developed by SWB[19,43] predicts about the same variations, but the contribution of the e_{aq}^- decay in reaction R1 is found to vary less (−1.13 to −0.36) with temperature.

3.1.2. Production and Fate of Hydroxyl Radicals. Overall, the yield of OH radicals increases linearly up to ~150 °C and then exhibits, while still increasing, a slight downward curvature as the temperature is further increased (Figure 1b). The three main reactions involved in the decay of OH are listed below in order of importance at 25 °C, the second reaction (R7) becoming predominant above ~100 °C (see Figure 2b):

$$e_{aq}^- + OH \rightarrow OH^-$$

$$\Delta g(OH) = -1.5 \text{ to } -0.2 \text{ from 25 to 300 °C} \quad \text{(R1)}$$

$$OH + OH \rightarrow H_2O_2$$

$$\Delta g(OH) = -1.24 \text{ to } -0.64 \text{ from 25 to 300 °C} \quad \text{(R7)}$$

$$H + OH \rightarrow H_2O$$

$$\Delta g(OH) = -0.44 \text{ to } -0.15 \text{ from 25 to 300 °C} \quad \text{(R8)}$$

Because all those reactions are partially diffusion-controlled with

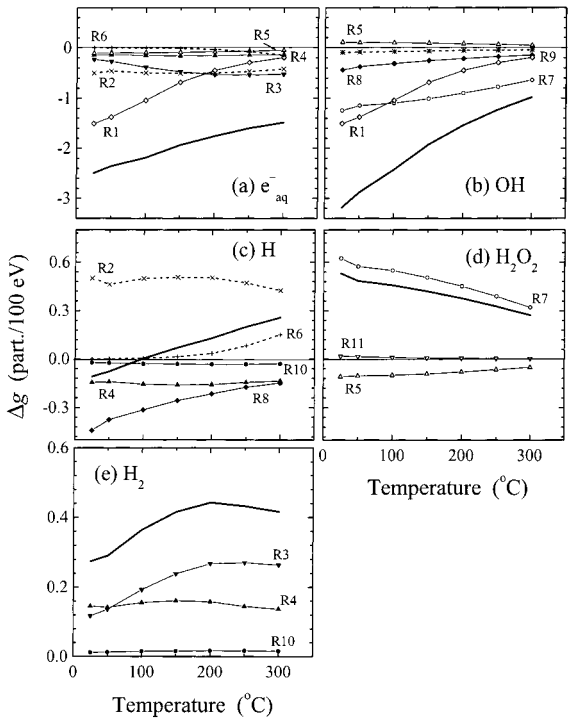

Figure 2. Contributions of the reactions listed in Table 2 in the cumulative yield variations Δg (in part./100 eV), over the range 10^{-12}–10^{-7} s, of (a) hydrated electrons, (b) OH radicals, (c) H atoms, (d) H_2O_2, and (e) molecular hydrogen, as a function of temperature. For the sake of clarity, the contributions of reactions R13 and R14 to g(OH) are not shown in the figure because they are lower than 0.06. In the case of reactions involving two identical species, the Δg-value that is shown accounts for the fact that each reaction eliminates two reactants. The bold solid lines represent, for each species, the sum of the contributions of all reactions that are involved in the decay or formation of the species in the considered time interval. The "initial" yields of the various species, that is, the yields that we have at $\sim 10^{-13}$ s before any reaction has occurred, are given in Table 3.

rate constants that vary less with temperature than the diffusion coefficients of the individual species, the decay of the OH radicals is reduced as the temperature increases.[41,42] As a consequence of this, more OH radicals are available to escape the spur and g(OH) increases with temperature, which is what we observe. According to the SWB model,[19,43] the self-reaction R7 remains predominant in the whole temperature range [Δg(OH) = −1.52 to −0.55 from 25 to 300 °C], whereas for reaction R1, Δg(OH) varies from −1.12 to −0.35. The contribution of reaction R8 is even less important (−0.18 to −0.066).

3.1.3. Production and Fate of Hydrogen Atoms. The four main reactions involved in the formation and decay of H atoms are listed below in order of importance at 25 °C (see Figure 2c):

$$e_{aq}^- + H^+ \rightarrow H$$
$$\Delta g(H) \approx 0.47 \text{ (nearly constant over all the temperature range)} \quad \text{(R2)}$$

$$H + OH \rightarrow H_2O$$
$$\Delta g(H) = -0.44 \text{ to } -0.15 \text{ from 25 to 300 °C} \quad \text{(R8)}$$

$$e_{aq}^- + H \rightarrow H_2 + OH^-$$
$$\Delta g(H) \approx -0.15 \text{ (nearly constant over all the temperature range)} \quad \text{(R4)}$$

$$e_{aq}^- + H_2O \rightarrow H + OH^-$$
$$\Delta g(H) = 0 \text{ to } 0.16 \text{ from 25 to 300 °C} \quad \text{(R6)}$$

Two of these reactions, reactions R8 and R6, are mostly responsible for the temperature dependence of g(H). A striking feature of the results is that reaction R6, whose contribution is negligible up to ∼150 °C, should not be neglected at higher temperatures. The overall effect is a linear increase in the H atom yield with temperature.

3.1.4. Production and Fate of Hydrogen Peroxide. The three main reactions involved in the formation and decay of H_2O_2 are listed below in order of importance at 25 °C (see Figure 2d):

$$OH + OH \rightarrow H_2O_2$$
$$\Delta g(H_2O_2) = 0.62 \text{ to } 0.32 \text{ from 25 to 300 °C} \quad \text{(R7)}$$

$$e_{aq}^- + H_2O_2 \rightarrow OH + OH^-$$
$$\Delta g(H_2O_2) = -0.11 \text{ to } -0.05 \text{ from 25 to 300 °C} \quad \text{(R5)}$$

$$H^+ + HO_2^- \rightarrow H_2O_2$$
$$\Delta g(H_2O_2) = 0.02 \text{ to } 0 \text{ from 25 to 300 °C} \quad \text{(R11)}$$

In the whole temperature range, hydrogen peroxide is formed mainly by the reaction R7 of the OH radical with itself. Moreover, the contributions of all those reactions decrease, in magnitude, almost linearly with increasing temperature. The overall effect is a linear decrease in the yield of H_2O_2 with temperature (Figure 1b).

3.1.5. Production of Molecular Hydrogen. The three main reactions involved in the formation of H_2 are listed below in order of importance at 25 °C, the second reaction R3 becoming predominant above 50 °C (see Figure 2e):

$$e_{aq}^- + H \rightarrow H_2 + OH^-$$
$$\Delta g(H_2) \approx 0.15 \text{ (nearly constant over all the temperature range)} \quad \text{(R4)}$$

$$e_{aq}^- + e_{aq}^- \rightarrow H_2 + 2OH^-$$
$$\Delta g(H_2) = 0.12 \text{ to } 0.26 \text{ from 25 to 300 °C} \quad \text{(R3)}$$

$$H + H \rightarrow H_2$$
$$\Delta g(H_2) \approx 0.015 \text{ (nearly constant over all the temperature range)} \quad \text{(R10)}$$

The only cumulative yield variation $\Delta g(H_2)$ which appreciably depends on temperature is that due to reaction R3: it increases linearly up to ∼150 °C and then remains almost constant above 200 °C. Although the $\Delta g(H_2)$ value resulting from reaction R4 is nearly constant over all the temperature range, a closer examination indicates in reality that it displays a small decrease with temperature above 200 °C (Figure 2e). The overall effect is a linear increase in the yield of H_2 with temperature and a slight decrease above 200 °C. This behavior contrasts somewhat with the experimental data of $g(H_2)$, which show a continuous increase over the range 25−300 °C (see Figure 1a).

The increase in $g(H_2)$ with temperature can be explained on the basis of the competition that takes place between intraspur reactions R3, R4, and R10, which are diffusion- or near-diffusion-controlled, and reaction R1, which is reactivity-controlled rather than diffusion-controlled.[41,42] Under those circumstances, the fraction of e_{aq}^- that is removed by reaction R1 becomes less as the temperature increases, which leads to more hydrated electrons available to either react in reactions

R3 and R4 (responsible for the majority of the H_2 yield) or escape into the bulk solution (see section 3.1.1). As a consequence of this, the overall effect is that the yields of e_{aq}^- and H_2 increase with temperature.

Our Monte Carlo simulations were used to quantitatively investigate such an explanation and showed that the situation is complex. First, the bimolecular reaction of e_{aq}^- involves Coulomb repulsion between two hydrated electrons, which increases with temperature due to the decrease of the dielectric constant of water (see section 2). This leads to the saturation of $\Delta g(H_2)$ due to reaction R3 above 200 °C (see Figure 2e). The sensitivity of $g(H_2)$ on this effect is discussed in section 3.2.1. Second, reaction R4 is not truly diffusion-controlled since its rate constant follows an Arrhenius relationship with an activation energy of 14 kJ/mol, which is less than that for self-diffusion in water.[27] That the temperature dependence of this reaction does not scale with that of self-diffusion of water could explain the decrease with temperature of the extent $\Delta g(H_2)$ for this reaction, as Figure 2e shows. Our simulations, which take into account those elements as realistically as possible, thus fail to fit satisfactorily the experimental data.

Much attention has been devoted in the literature to understanding the experimental steady increase of $g(H_2)$ with temperature, but the question remains open. To reproduce this result quantitatively, SWB[19] assumed that the efficiency of one of the dissociation decay channels for excited water molecules, namely, $H_2O^* \rightarrow H_2 + O(^1D)$,[44] was temperature-dependent, so that the initial yield of H_2 (before "contact reactions") increases with temperature. The authors founded their assumption on the diminution of hydrogen bonding in liquid water at high temperatures, which could possibly lead to a decrease of the so-called "cage recombination" of geminate pairs.[19] However, they did not put forward any physical mechanism that would justify such a possible change in the temperature dependence of the *relative* contributions of the various dissociative decay channels for H_2O^*. In the present study, we explore two alternative explanations and test them through our Monte Carlo simulations. The first one consists of accounting for the screening of the Coulomb forces between the two hydrated electrons in reaction R3, whereas the second one involves the possible temperature dependence of the electron thermalization distances (see sections 3.2.1 and 3.3, respectively).

3.2. Sensitivity of the Results to Reaction Rate Constants. Due to scarce or even contradictory experimental data, the curves giving the temperature dependence of several of the reaction rate constants that intervene in the calculations are not precisely known. In some cases, very different curves can equally fit the experimental data, so that there is a large uncertainty in the rate constant values at high temperatures. For this reason, it was important to estimate the impact of this uncertainty on the calculated radiolytic yields. In addition, by comparing those results to experiment, it is also possible to determine what the temperature dependence of a given reaction rate constant may be.

3.2.1. $e_{aq}^- + e_{aq}^-$ Reaction. The data relative to the bimolecular self-reaction of the hydrated electron are unusual in two respects: (i) the lack of any ionic strength dependence, as was demonstrated by Schmidt and Bartels[45] at room temperature and (ii) the abrupt drop in the value of the rate constant above 150 °C, as reported by Christensen and Sehested[46] (hereafter referred to as CS).

The lack of ionic strength effect in the disproportionation reaction of e_{aq}^- could indicate that each hydrated electron sees a screened Coulomb interaction from the other e_{aq}^- and that consequently Coulomb forces are overestimated in reaction R3. In the limiting situation where the Coulomb interaction between the two e_{aq}^- would not perturb at all this reaction, the temperature dependence of the rate constant k_3 could be modeled by the Smoluchowski equation (eq 3), which applies to diffusion-controlled reactions where Coulomb forces do not come into play (see section 2). This reaction rate constant was introduced in our Monte Carlo simulations. The resulting *g*-values obtained for the "reducing" species e_{aq}^-, H, and H_2 in the range 25−300 °C are shown in Figures 3a−3c, where they are compared with experiment and with the yields computed with $k_3(T)$ modeled by the Debye equation (eqs 4 and 5; see Figure 1a). It can be seen that, when Coulomb forces are not taken into account, $g(H_2)$ and $[g(H) + g(H_2)]$ are enhanced, and $g(e_{aq}^-)$ is diminished. The largest effect is obtained for $g(H_2)$, which no longer decreases at elevated temperatures and now matches the experimental data quite well (Figure 3b).

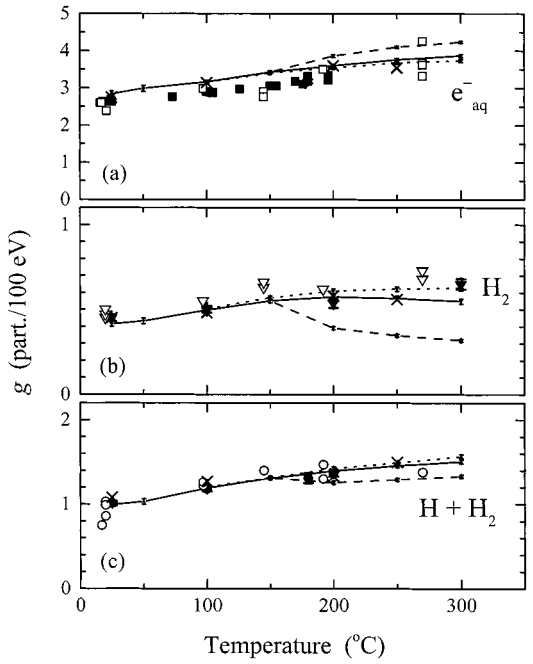

Figure 3. Sensitivity of our Monte Carlo simulations to the temperature dependence of the rate constant (k_3) for the bimolecular reaction of e_{aq}^- (reaction R3). The different simulated yield results (in part./100 eV) at 10^{-7} s for (a) $g(e_{aq}^-)$, (b) $g(H_2)$, and (c) $[g(H) + g(H_2)]$ over the range 25−300 °C, obtained for three selected temperature dependences of $k_3(T)$, are shown as the following lines: - - - - -, $k_3(T)$ modeled by the Smoluchowski equation (eq 3); —, $k_3(T)$ modeled by the Debye equation (eqs 4 and 5); and - - -, $k_3(T)$ as determined by Christensen and Sehested (ref 46). The error bars show the 95% confidence intervals of the simulation results. Symbols, representing experimental data, are the same as in Figure 1.

The results of CS,[46] who reported an abrupt drop in the rate constant of reaction R3 above 150 °C, need to be confirmed, as they may be a function of the pH of the solution[27,41] and as CS[46] obtained their data under alkaline conditions. Diffusion−kinetic modeling calculations[26] of the spur reactions in near-neutral pH solutions suggest that such an abrupt change does not occur because when it is incorporated in the model, a sharp downward discontinuity in $g(H_2)$ is predicted, which is not observed experimentally. Moreover, SWB[19] reported that when they use the data of CS[46] for reaction R3 in their spur diffusion model, the calculated temperature-dependent *g*-values for e_{aq}^-, H, and H_2 show a characteristic inflection at 150 °C that is also not observed experimentally.

Assuming that the rate constant of the disproportionation reaction of e^-_{aq} determined by CS[46] is valid for neutral pH water up to 150 °C, its value at higher temperatures had to be extrapolated.[27] Unfortunately, CS[46] assumed in their analysis of the kinetic data that the molar extinction coefficient of e^-_{aq} at its absorption maximum was constant with temperature, whereas Elliot and Ouellette[41] later found that it decreases with temperature and so corrected the temperature dependence of the rate constant reported for this reaction. Up to 150 °C, the corrected data obey the Arrhenius relationship with an activation energy of 20.3 kJ/mol.[27,41] Assuming that reaction R3 is diffusion-controlled, extrapolation of these data above 150 °C has been modeled using the Debye equation (eqs 4 and 5).[27] Except when otherwise stated, this modeled rate constant was used in our Monte Carlo simulations over the whole temperature range.

When the rate constant $k_3(T)$ thus modeled was incorporated in their calculations, SWB[19] no longer observed an inflection at 150 °C in the yields for e^-_{aq}, H, and H_2. However, to explain the observed increase in $g(H_2)$ above 200 °C, these authors included a temperature-dependent source of H_2, generated from the fragmentation channel of H_2O^* into $H_2 + O(^1D)$ during the physicochemical stage (see section 3.1.5). The temperature dependence of $g(H_2)$ formed by this latter process was determined so that the total H_2 yield fitted the experimental data. There is, accordingly, no surprise that SWB[19] do not observe a decrease in $g(H_2)$ at elevated temperatures and correctly reproduce the linear increase exhibited by the experimental data.

To confirm the findings of deterministic spur diffusion−kinetic models, the temperature dependence of $k_3(T)$ as determined by CS[46] in the range 25−300 °C was incorporated in our Monte Carlo simulations. The resulting simulated *g*-values for e^-_{aq}, H, and H_2 are shown in Figure 3. While the calculated yields of the "oxidizing" species, $g(OH)$ and $g(H_2O_2)$, hardly change (within implied uncertainties; results not shown here), $g(e^-_{aq})$, $g(H_2)$, and $[g(H) + g(H_2)]$ are strongly influenced by the abrupt drop in $k_3(T)$ around 150 °C; at this point, they suddenly deviate sharply from experiment and also from the simulated yields obtained with the rate constant $k_3(T)$ modeled either by the Smoluchowski equation or by the Debye equation. In contrast to $g(H_2)$ and $[g(H) + g(H_2)]$, which show sharp downward discontinuities, $g(e^-_{aq})$ is enhanced above 150 °C. As one can see, simulated $g(H_2)$ values are well below the experimental data, which confirms that the $k_3(T)$ values reported by CS[46] are inappropriate in near-neutral pH water at temperatures above ∼150 °C.[48]

3.2.2. $e^-_{aq} + H^+$ Reaction. The rate constant $k_2(T)$ for the reaction of e^-_{aq} with the proton (reaction R2) has been investigated in aqueous solution between 25 and 250 °C by Shiraishi et al.[47] and Elliot et al.[27,28] The Arrhenius plot of the data reported by Elliot[27] does not exhibit the concave upward curvature observed by Shiraishi et al.[47] in the temperature region above 150 °C. In the present paper, we determined the sensitivity of our simulated yield results on variations in the value of the rate constant for this reaction. The resulting calculated *g*-values for e^-_{aq}, OH, H_2, and H, for both reported temperature dependences of k_2, are compared with the experimental data in Figure 4. As can be seen, $g(OH)$ and $g(H_2)$, as well as $g(H_2O_2)$ (not shown here), are found to be rather insensitive to this parameter over the whole temperature range. As expected, when the temperature dependence for the rate constant as determined by Shiraishi et al.[47] is used, $g(e^-_{aq})$ presents a downward curvature, instead of a steady increase, and $[g(H) + g(H_2)]$ increases much faster with temperature than what is observed experimentally.

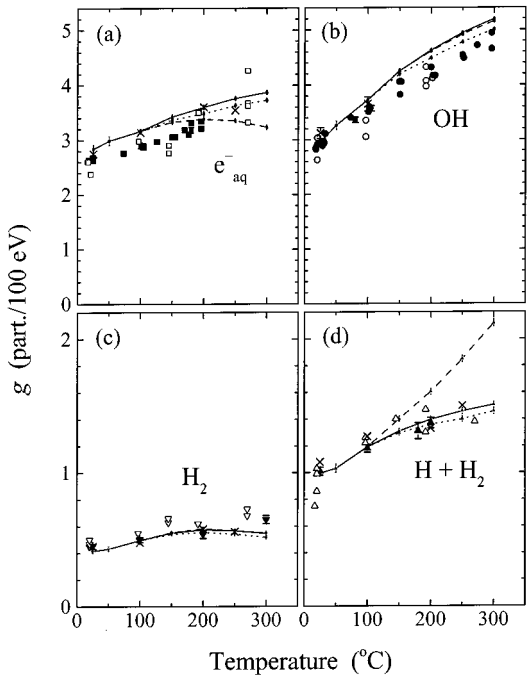

Figure 4. Sensitivity of our Monte Carlo simulations to the temperature dependence of the rate constants (k_1 and k_2) of reactions R1 and R2. Simulated yield results (in part./100 eV) at 10^{-7} s for (a) $g(e^-_{aq})$, (b) $g(OH)$, (c) $g(H_2)$, and (d) $[g(H) + g(H_2)]$ over the range 25−300 °C are shown as the following lines: —, $k_1(T)$ modeled by the Noyes equation (eq 2) using a negative activation energy (−3.5 kJ/mol) and $k_2(T)$ as determined by Elliot (ref 27); - - -, $k_1(T)$ modeled by the Noyes equation (eq 2) using a negative activation energy (−3.5 kJ/mol) and $k_2(T)$ as determined by Shiraishi et al. (ref 47); and ....., $k_1(T)$ modeled by an Arrhenius relationship with an apparent activation energy of 7.92 kJ/mol and $k_2(T)$ as determined by Elliot (ref 27). The error bars show the 95% confidence intervals of the simulation results. Symbols, representing experimental data, are the same as in Figure 1.

In consequence, the use of the temperature dependence of k_2 as reported by Elliot[27] seems to be justified, judging from the good agreement obtained between simulations and experiment.

3.2.3. e^-_{aq} + OH Reaction. The rate constant (k_1) for the reaction of hydrated electrons with hydroxyl radicals (reaction R1), which was studied by Elliot and Ouellette,[41] could only be estimated up to 150 °C. These data could be fitted to eq 2 by using a negative activation energy (−3.5 kJ/mol), but the fit was not convincing.[27] However, as they stand, the data could also be fitted to an Arrhenius relationship with an apparent activation energy of 7.92 kJ/mol; in this case, the rate constant value at 300 °C is $k_1 = 1.4 \times 10^{11}$ M^{-1} s^{-1} instead of 6.3×10^{10} M^{-1} s^{-1} when the Noyes equation is used to fit the experimental data.[27,41] As it is possible that reaction R1 is one of those hydrated electron reactions where the temperature dependence of the rate constant actually decreases gradually with temperature above a certain temperature,[49] the Arrhenius fit must be considered an upper bound for temperatures above 150 °C.[27] As before, the sensitivity of our simulated yield results on variations in the value of k_1 can here be determined. Both fits for $k_1(T)$ were incorporated into our Monte Carlo simulations, and the yields so obtained are compared with the experimental data in Figure 4. If the calculated values of $g(H_2O_2)$ (not shown here) are found to be insensitive to this parameter over the range 25−300 °C, it can be seen in the figure that those of $g(e^-_{aq})$, $g(OH)$, $g(H_2)$, and $[g(H) + g(H_2)]$ are all slightly diminished when the Arrhenius fit is introduced in the simulations, but not enough to determine which temperature

dependence for k_1 should give the better fit. Throughout this article, $k_1(T)$ was modeled by the Noyes equation (eq 2).

3.3. Sensitivity of the Results to the Temperature Dependence of Electron Thermalization Distances. Based on the simple relation $MFP = 1/(\sigma N)$ already discussed in section 2, if scattering cross sections of subexcitation electrons were constant, then their thermalization distances would be inversely proportional to the density of pressurized water, which decreases with increasing temperature. However, because the degree of structural order diminishes as the temperature of water is increased, the scattering cross sections of subexcitation electrons are expected to increase with temperature,[10,17,20,21] resulting in a *decrease* of electron thermalization distances. It is difficult to estimate to what extent order might affect thermalization distances, but this effect could be strong enough to reduce those distances significantly.

Different temperature dependences for the electron thermalization distances (r_{th}) were therefore incorporated into our simulations to determine their impact on the radiolytic yields. Besides the reference case (b) where r_{th} values were kept constant with temperature (t), three other temperature dependences (a, c, and d) were tested, namely:

(a) $r_{th}(t) = r_{th}(25\ °C)\dfrac{\rho(25\ °C)}{\rho(t)}$, where ρ is the density of water

(b) $r_{th}(t) = r_{th}(25\ °C)$

(c) $r_{th}(300\ °C) = \dfrac{r_{th}(25\ °C)}{2}$, $r_{th}(t)$ decreasing linearly with t

(d) $r_{th}(300\ °C) = \dfrac{r_{th}(25\ °C)}{4}$, $r_{th}(t)$ decreasing linearly with t

In the case (a), no structural order effect was assumed, so that r_{th} values are only affected by the variations in water density (see section 2). For the other cases (b−d), order affects in varying degree thermalization distances. For the cases (c) and (d), the resulting temperature dependences for r_{th} were assumed to vary linearly with t.

Our simulated results are shown in Figure 5 for $g(e_{aq}^-)$, $g(H_2)$, and $[g(H) + g(H_2)]$ only, since the calculated yields $g(OH)$ and $g(H_2O_2)$ are found to be insensitive to the temperature dependence of r_{th} over the studied range 25−300 °C. When thermalization distances increase with temperature, instead of being constant, $g(e_{aq}^-)$ is enhanced whereas $g(H_2)$ and $[g(H) + g(H_2)]$ are diminished at higher temperatures. As can be seen in Figure 5, experimental data for $g(e_{aq}^-)$ and $g(H_2)$ are better reproduced if r_{th} values decrease with increasing temperature, the temperature dependence (c) appearing to give the best fits. For $[g(H) + g(H_2)]$, all simulated curves are almost appropriate and describe the experimental data reasonably well. The present simulation results seem therefore to indicate that inclusion of a temperature effect in r_{th}, and therefore in the low-energy electron scattering cross sections, to account for the loss of structural order in liquid water as temperature increases, offers a better agreement of the calculated radiolytic yields with experiment.

LaVerne and Pimblott[26] have performed deterministic diffusion−kinetic model calculations to show how scaling of the radii of the initial spatial distributions of the various reactive species with temperature affects the calculated g-values. As these authors pointed out, the temperature dependence of the initial

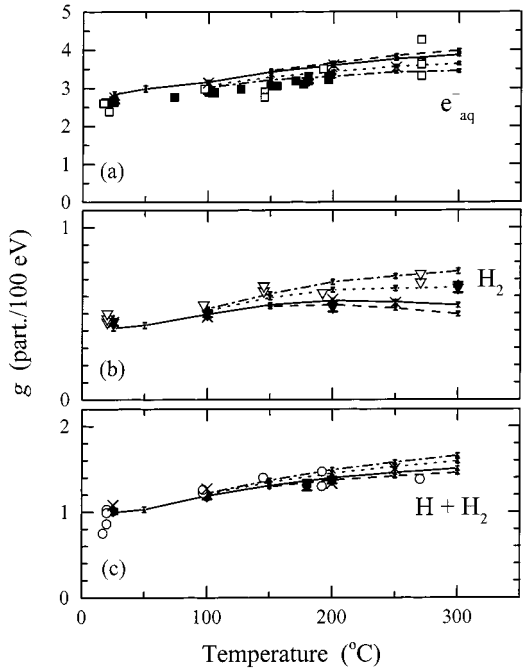

Figure 5. Sensitivity of our Monte Carlo simulations to the temperature dependence of electron thermalization distances (r_{th}). Simulated yield results (in part./100 eV) at 10^{-7} s for (a) $g(e_{aq}^-)$, (b) $g(H_2)$, and (c) $[g(H) + g(H_2)]$ over the range 25−300 °C, are shown as the following lines: —, $r_{th}(t) = r_{th}(25\ °C)$ = constant; - - -, $r_{th}(t) = r_{th}(25\ °C)$ $[\rho(25\ °C)/\rho(t)]$, where $\rho(t)$ is the density of water at the temperature t (in degrees Celsius); - - - - - -, $r_{th}(300\ °C) = r_{th}(25\ °C)/2$, r_{th} decreasing linearly with t; and — - — - — -, $r_{th}(300\ °C) = r_{th}(25\ °C)/4$, r_{th} decreasing linearly with t. The error bars show the 95% confidence intervals of the simulation results. Symbols, representing experimental data, are the same as in Figure 1.

distribution of e_{aq}^- is determined by the distance the secondary electron travels until it is hydrated (that is, by the thermalization distance), which may well be strongly temperature-dependent. Their best fit to experiment was obtained for an activation-controlled increase of the initial spur radius of the hydrated electron (r^o_e) from 2.3 nm at 25 °C to 5.8 nm at 300 °C and a temperature-independent initial spur radius for all the other species (r^o), which is kept at 0.85 nm.[26]

Swiatla-Wojcik and Buxton[19] have also scaled the initial spur radii r^o_e and r^o, respectively, of e_{aq}^- and of the other species (H^+, H, OH, H_2, and H_2O_2), with temperature. In their calculations, instead of having $r^o_e(t)$ proportional to the inverse of the density $\rho(t)$ (see section 2), they used a law in $[\rho(t)]^{-1/3}$. The values of $r^o_e(25\ °C)$ and $r^o(25\ °C)$ were obtained, for each initial spatial distribution function (Gaussian, exponential, and central minimum) considered by the authors, by fitting the calculated g-values to the observed ones at 25 °C. For the Gaussian distribution, for example, the best fit was found with $r^o_e = 2.3$ nm and $r^o = 0.85$ nm,[19] the same values as those used by LP.[26] SWB[19] further noted that the use of a law in $[\rho(t)]^{-1/3}$ for $r^o_e(t)$ results in r^o_e values increasing by no more than 11.5% up to 300 °C, compared with more than 150% in the model employed by LP.[26]

Our result that electron thermalization distances should decrease with increasing temperature is in contradiction to that of spur model studies. However, according to our findings, the most sensitive parameter to the temperature dependence of r_{th} is $g(H_2)$. As already mentioned, LP[26] largely underestimated $g(H_2)$ above 150 °C due to the use of CS data[46] for the rate constant of the disproportionation reaction of e_{aq}^- (reaction R3). Fortunately, they chose to rely on $g(e_{aq}^-)$ to determine the

temperature dependence of r_{th}. To account for an observed increase of $g(e^-_{aq})$ of ~40% from 25 to 300 °C, these authors had to increase r_{th} by more than 150%.[26] Their need for such a large increase in r_{th} is due to the fact that they underestimated $g(e^-_{aq})$ at elevated temperatures. Indeed, as pointed out by SWB,[19] LP[26] assumed that the reaction between e^-_{aq} and OH is diffusion-controlled, whereas it is now known to be activation-controlled.[27,41] As this reaction is an important reaction in the spur, the use of the correct temperature dependence of the rate constant is expected to change the results.

In fact, LP[26] made some trial calculations in which the rate constants for reactions R1 and R4 were scaled using an Arrhenius equation with an activation energy of 12.6 kJ/mol[50] instead of the self-diffusion in water (~15.5 kJ/mol). They found that there is no observable effect on $g(H_2)$ and $g(H_2O_2)$, whereas the yields of e^-_{aq} and OH radicals are increased by about 0.25 at 300 °C. These authors[26] also reported that, at 300 °C, the activation-energy-scaled rate constants of reactions R1 and R4 are 60% of those obtained by scaling to the self-diffusion in water. However, the rate constant value at 300 °C, recommended by Elliot,[27] $k_1 = 6.3 \times 10^{10}$ M^{-1} s^{-1} (see section 3.2.3), is ~9.5 times smaller than the diffusion-controlled value used by LP.[26]

We can, therefore, roughly estimate that the value of $g(e^-_{aq}) \approx 2.5$ calculated by LP[26] for the temperature-independent initial spur radius $r^o_e = 2.3$ nm was probably underestimated by about 1.4 at 300 °C. This is consistent with the extent $\Delta g(e^-_{aq})$ of reaction R1, which decreases (in absolute value) by ~1.3 between 25 and 300 °C (see section 3.1.1 and Figure 1a) instead of remaining approximately constant for a diffusion-controlled reaction. This also explains why g(OH) is greatly affected by variations in the value of r^o_e in the LP model (increase of ~0.57 for a 150% increase in r^o_e),[26] which is in disagreement with our finding (increase of ~0.04 for a 100% increase in r_{th}). In fact, in our case, reaction R1 is completely quenched at 300 °C, so that the same relative variation in the Δg value of this reaction has little impact on g(OH) and $g(e^-_{aq})$. On that account, we find that about 70% of the variations of $g(e^-_{aq})$ induced by a decrease in r_{th} comes from reactions of e^-_{aq} with itself (reaction R3), whereas about 15% and 10% come from reactions of e^-_{aq} with OH radicals (reaction R1) and H atoms (reaction R4), respectively. This is not the case for LP,[26] since reaction R3 is completely quenched at 300 °C due to the use of CS data.[46]

Since SWB[19] have introduced a temperature-dependent initial yield of H_2 to fit the experimental $g(H_2)$ values above 200 °C (see sections 3.1.5 and 3.2.1) and since the remaining radiolytic yields are probably not sensitive enough to discriminate between a slight increase of r^o_e with temperature (11.5% up to 300 °C) and a 50% decrease, their model predictions should not be sensitive enough to determine the temperature dependence of the radius of the initial spatial distribution of e^-_{aq} within the spur.

3.4. Time Decays of e^-_{aq} and OH Radicals as a Function of Temperature. Figures 6 and 7b show, respectively, the results of our Monte Carlo calculations for the time-dependent yields of OH radicals and of hydrated electrons, over the range 10^{-12}–10^{-6} s, assuming that electron thermalization distances do not depend on temperature. Due to the fact that "contact reactions" are less important when the density of water is smaller, the yields of both OH radicals and e^-_{aq} at ~10^{-12} s (after "contact reactions" have been allowed to take place) slightly increase as temperature increases (see Table 3). After ~10^{-11} s, both g(OH) and $g(e^-_{aq})$ start decreasing with time. As discussed in previous sections, the reactions making the largest contributions in the OH and e^-_{aq} yield decays (reactions R1, R2, R3, R7, and R8) occur generally *less* as temperature is increased (see Figures 2a and 2b), so that g(OH) and $g(e^-_{aq})$ decay less rapidly at higher temperature. After ~10^{-7} s, the yield of hydrated electrons decreases dramatically at high temperatures

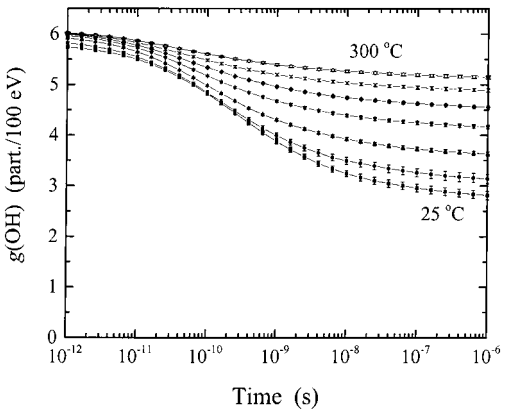

Figure 6. Time decay of OH radicals for the radiolysis of liquid water at 25, 50, 100, 150, 200, 250, and 300 °C, in the time interval 10^{-12}–10^{-6} s. Simulated yield results are obtained from averages over 150 tracks of 300-MeV protons (average LET ~ 0.3 keV/μm) (except at 25 and 50 °C where the simulated number of proton tracks is 40). The error bars show the 95% confidence intervals of the simulation results. In the simulations, electron thermalization distances (r_{th}) are taken as constant over the whole temperature range and equal to r_{th}(25 °C). Note that there are, at present, no experimental data reported for the temporal variation of g(OH) at high temperatures with which to compare our results.

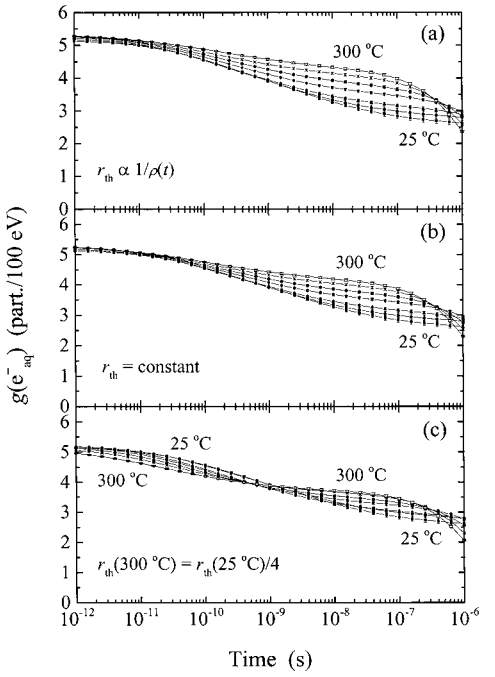

Figure 7. Sensitivity of the time decay of hydrated electrons at 25, 50, 100, 150, 200, 250, and 300 °C, in the time range 10^{-12}–10^{-6} s, to the temperature dependence of electron thermalization distances (r_{th}): (a) $r_{th}(t) = r_{th}(25\ °C)$ [$\rho(25\ °C)/\rho(t)$], where $\rho(t)$ is the density of water at the temperature t (in degrees Celsius); (b) $r_{th}(t) = r_{th}(25\ °C)$ = constant; and (c) $r_{th}(300\ °C) = r_{th}(25\ °C)/4$, r_{th} decreasing linearly with t. Note that, for the sake of comparison, the r_{th} values at 25 °C are taken to be the same for the three considered cases, so that the temporal variation of $g(e^-_{aq})$ at 25 °C can be viewed as a reference curve, identical in the three figures. The error bars show the 95% confidence intervals of the simulation results. There are at present no experimental data reported for the temporal variation of $g(e^-_{aq})$ at high temperatures with which to compare our results.

TABLE 3: Calculated Yields (in part./100 eV) of the Various Species Present at $\sim 10^{-13}$ s ("Initial" Yields) and at $\sim 10^{-12}$ s (After "Contact Reactions" Have Been Allowed to Take Place) Obtained from Our Monte Carlo Simulations of Short ($\sim$100 μm) Track Segments of 300-MeV Protons (Average LET $\sim$ 0.3 keV/μm) in Liquid Water, over the Range 25−300 °C

	t (°C)	$g(e_{aq}^-)$	g(H)	$g(H_2)$	g(OH)	$g(H_2O_2)$
"initial" yields	25−300	5.36	0.72	0.14	6.11	0.062
after "contact reactions", at $\sim 10^{-12}$ s	25	5.13	0.55	0.19	5.74	0.092
	300	5.24	0.65	0.20	6.02	0.071

(above 150−200 °C), due to the reactions of e_{aq}^- with H_2O and with H^+ ions homogeneously distributed in the solution (see top of section 3).

Figures 7a−7c display the influence of the temperature dependence of r_{th} on the time-dependent yields of e_{aq}^-, in the range $10^{-12}-10^{-6}$ s. It should be noted that the values of r_{th} at 25 °C are taken to be the same for the three figures, whereas they increase with temperature in Figure 7a, remain constant (at their 25 °C values) in Figure 7b, and decrease in Figure 7c. This latter figure shows that, due to the decrease in r_{th}, the decay of $g(e_{aq}^-)$ at 300 °C starts earlier than what is observed at 25 °C. As a consequence, the set of decay kinetics of e_{aq}^- obtained in this case (Figure 7c) significantly differs from the other two sets (Figures 7a and 7b). The earlier start of the e_{aq}^- decay kinetics is expected since a decrease in thermalization distances implies that electrons get hydrated closer to the other reactive species; as a result, (i) less time for diffusion is required before encounters occur and (ii) encounters are more probable so that more intraspur reactions involving e_{aq}^- take place. Indeed, as can be seen in Figure 7c, at subnanosecond times, $g(e_{aq}^-)$ decreases with increasing temperature. There is subsequently a reversal of behavior, the $g(e_{aq}^-)$ decay curve obtained at 300 °C crossing above the corresponding curve at 25 °C around 10^{-9} s. Hence, in the time interval $\sim 10^{-9}-10^{-7}$ s, $g(e_{aq}^-)$ increases as temperature is increased. Unfortunately, there are at present no data reported for the decay of e_{aq}^- at high temperatures with which to compare our results.

Based on these results, it appears that experimental studies on the time dependence of $g(e_{aq}^-)$ as a function of temperature would be most valuable as they could give information on the temperature dependence of r_{th}. Indeed, electron thermalization distances in liquid water at 25 °C used in this work[10,17] were scaled so that the time dependence of the yield of hydrated electrons fitted the available experimental data[27,35,51−53] between $\sim$30 ps and 10^{-6} s.[54] Given experimental data, such a scaling could therefore be applied at different temperatures to determine the temperature dependence of r_{th}.

Swiatla-Wojcik and Buxton[19] also studied the time-dependent yields of e_{aq}^- and of OH radicals as a function of temperature. Their results for the hydroxyl radical are in good agreement with those obtained here (Figure 6). As for the e_{aq}^- yield decay curves, they are similar to those presented in Figure 7c, which correspond to the case of decreasing electron thermalization distances as temperature increases. This could be due to the fact that the r_{th} values used by SWB[19] remain small at elevated temperatures (see section 3.3). It should also be noted that reactions of e_{aq}^- with the medium have not been incorporated in the model developed by SWB,[19] so $g(e_{aq}^-)$ does not decrease at high temperatures between $\sim 10^{-7}$ and 10^{-6} s (see top of section 3).

LaVerne and Pimblott[26] have also examined the time-dependent yields of hydrated electrons as a function of temperature for three types of spurs: (i) "Type-1 spur" where all initial spur radii are kept constant at their 25 °C values (r^o_e = 2.3 nm, r^o = 0.85 nm, see section 3.3); (ii) "Type-2 spur" where all initial spur radii are temperature-scaled according to the self-diffusion in water (r^o_e (300 °C) = 10.0 nm, r^o (300 °C) = 3.7 nm); and (iii) "Type-5 spur" where the radius of the initial spatial distribution of e_{aq}^- is determined by an Arrhenius-like scaling [r^o_e (300 °C) = 5.8 nm] and the radii of all the other reactive species are kept constant. These three different types of spurs give very different temporal variations of $g(e_{aq}^-)$. For a type-1 spur, $g(e_{aq}^-)$ decreases with increasing temperature over most of the time range studied, but for temperatures greater than 150 °C, less e_{aq}^- decay is observed after $\sim 10^{-9}$ s, so that $g(e_{aq}^-)$ exhibits a minimum around 150 °C. This is due to the quenching of the self-reaction of the hydrated electron resulting from the use of CS data[46] for the rate constant of this reaction (see section 3.2.1). Changing the radii from a type-1 to type-2 spur completely reverses the relative temperature dependence of $g(e_{aq}^-)$ at subnanosecond times; for a type-2 spur, $g(e_{aq}^-)$ increases with increasing temperature over the whole time range. A type-5 spur gives results similar to that of a type-2 spur, except that the variations of the computed yields with temperature are somewhat less pronounced. As already mentioned, at 300 °C, the decrease in the initial spur radius of hydrated electrons from 10.0 nm (type-2) to 5.8 nm (type-5) leads to a faster e_{aq}^- decay kinetics and a larger decrease of $g(e_{aq}^-)$ with time.

4. Conclusions

In this paper, Monte Carlo simulations were used to investigate the effects of temperature on the primary yields (g-values) of the radical and molecular products of the radiolysis of pure, deaerated liquid water over the range 25−300 °C. To reproduce the effects of ^{60}Co γ-radiolysis, the initial energy deposition (prior to 10^{-14} s) was approximated by considering short segments ($\sim$100 μm) of 300-MeV proton tracks, corresponding to an average LET obtained in the simulations of $\sim$0.3 keV/μm. The independent reaction times (IRT) approximation was subsequently used to simulate the nonhomogeneous chemical evolution of the various reactive species formed in these tracks at the end of the physicochemical stage ($\sim 10^{-12}$ s). Our g-values for the "reducing" (e_{aq}^-, H, and H_2) and "oxidizing" (OH and H_2O_2) radiolytic species, calculated at 10^{-7} s after the ionizing event, suggest an increase in $g(e_{aq}^-)$, g(OH), and [g(H) + $g(H_2)$] and a decrease in $g(H_2O_2)$ with increasing temperature, in agreement with most of the available experimental data over the whole range of temperature.

The sensitivity of our calculated g-values to the rate constant values of the most important spur reactions and to the temperature dependence of electron thermalization distances was also examined. We confirmed, in particular, that the temperature dependence of the bimolecular self-reaction of e_{aq}^- as reported by Christensen and Sehested[46] is inappropriate in near-neutral pH water at temperatures above 150 °C. The present calculations show that the yields of e_{aq}^-, H, and H_2 are dependent on the thermalization distances of subexcitation electrons. The best agreement with experiment is found to occur when the distances of electron thermalization *decrease* with increasing temperature, a result that is at variance with the predictions of previous deterministic diffusion−kinetic modeling studies.[19,26] Physically, such a decrease in r_{th} as the temperature increases could be linked to an increase in the scattering cross sections of subexcitation electrons that would account for the corresponding

decrease in the degree of structural order of water molecules due to the increasing breaking of hydrogen bonds with temperature.

The impact of the lack of ionic strength effect in the bimolecular self-reaction of e_{aq}^- has also been estimated by modeling the temperature dependence of the rate constant k_3 by the Smoluchowski equation, which applies to diffusion-controlled reactions where Coulomb forces do not play any role. Results of simulations show that the variations of the *g*-values with temperature, and especially that of $g(H_2)$, are better described in the case where the screening of the Coulomb forces between the two e_{aq}^- in the disproportionation reaction of the hydrated electron is taken into consideration.

Finally, the time-dependent yields of e_{aq}^- and OH radicals have been given as functions of temperature, in the range 10^{-12}–10^{-6} s. The major conclusion to be drawn here is that the temporal variation of $g(e_{aq}^-)$ at elevated temperatures is sensitive to the temperature dependence of r_{th}. Experimental studies of the decay of hydrated electrons as functions of time and temperature could therefore be a very useful source of information on the thermalization of subexcitation electrons.

The good overall accord of our calculated yield values with the experimental data available from the literature demonstrates that Monte Carlo simulation methods offer a most promising avenue at present to further develop our understanding of temperature effects in the radiolysis of water. Currently, work is in progress at our laboratory to calculate the *g*-values in liquid water as a function of temperature and for a variety of LET, using those simulation techniques.

Acknowledgment. The authors are indebted to Dr. A. John Elliot of Atomic Energy of Canada Limited, Chalk River Laboratories, for a number of helpful and stimulating discussions and for providing his experimental data prior to publication. The work described herein was supported by the Canadian Institutes of Health Research and the Natural Sciences and Engineering Research Council of Canada, and, in part, by the Atomic Energy of Canada Limited (AECL Contract No. UC-568). The support of the France–Québec Cooperation Program in Medical Research in the form of a visiting grant to one of us (Ph.B.) is also gratefully acknowledged.

References and Notes

(1) Cohen, P. *Water Coolant Technology of Power Reactors*; American Nuclear Society: La Grange Park, Illinois, 1980.

(2) *CRC Handbook of Radiation Chemistry*; Tabata, Y., Ito, Y., Tagawa, S., Eds.; CRC Press: Boca Raton, Florida, 1991; p 785.

(3) Buxton, G. V. *Proceedings of the 5th International Conference on Water Chemistry of Nuclear Reactor Systems*; British Nuclear Energy Society: London, 1989; p 123. See also Buxton, G. V. *Int. J. Radiat. Biol.* **1991**, *59*, 1.

(4) Hickel, B. *J. Chim. Phys.* **1991**, *88*, 1177.

(5) Woods, R. J.; Pikaev, A. K. *Applied Radiation Chemistry: Radiation Processsing*; Wiley: New York, 1994; p 490.

(6) McCracken, D. R.; Tsang, K. T.; Laughton, P. J. *Aspects of the Physics and Chemistry of Water Radiolysis by Fast Neutrons and Fast Electrons in Nuclear Reactors*; Report AECL-11895; 1998.

(7) Burns, W. G.; Moore, P. B. *Radiat. Eff.* **1976**, *30*, 233.

(8) Spinks, J. W. T.; Woods, R. J. *An Introduction to Radiation Chemistry*, 3rd ed.; Wiley: New York, 1990; p 243.

(9) Ferradini, C.; Jay-Gerin, J.-P. *Can. J. Chem.* **1999**, *77*, 1542.

(10) Cobut, V.; Frongillo, Y.; Patau, J. P.; Goulet, T.; Fraser, M.-J.; Jay-Gerin, J.-P. *Radiat. Phys. Chem.* **1998**, *51*, 229.

(11) Frongillo, Y.; Goulet, T.; Fraser, M.-J.; Cobut, V.; Patau, J. P.; Jay-Gerin, J.-P. *Radiat. Phys. Chem.* **1998**, *51*, 245.

(12) Frongillo, Y.; Goulet, T.; Fraser, M.-J.; Bernat, Ph.; Jay-Gerin, J.-P.; Elliot, A. J. *Book of Abstracts, Journées d'Études de Chimie sous Rayonnement*, Orléans–Nouan-le-Fuzelier, France, 19–24 mai 1996; p C-2.

(13) Platzman, R. L. *Radiat. Res.* **1955**, *2*, 1. Weiss, J. *J. Chim. Phys.* **1955**, *52*, 539.

(14) Cobut, V.; Frongillo, Y.; Jay-Gerin, J.-P.; Patau, J. P. *Radiat. Phys. Chem.* **1992**, *40*, 589.

(15) Mozumder, A. *Fundamentals of Radiation Chemistry*; Academic Press: San Diego, 1999; p 271.

(16) Goulet, T.; Jay-Gerin, J.-P. *J. Phys. Chem.* **1988**, *92*, 6871. Goulet, T.; Jay-Gerin, J.-P. *Radiat. Res.* **1989**, *118*, 46. Goulet, T.; Patau, J. P.; Jay-Gerin, J.-P. *J. Phys. Chem.* **1990**, *94*, 7312.

(17) Goulet, T.; Jay-Gerin, J.-P.; Frongillo, Y.; Cobut, V.; Fraser, M.-J. *J. Chim. Phys.* **1996**, *93*, 111.

(18) Rowntree, P.; Parenteau, L.; Sanche, L. *J. Chem. Phys.* **1991**, *94*, 8570. Cobut, V.; Jay-Gerin, J.-P.; Frongillo, Y.; Patau, J. P. *Radiat. Phys. Chem.* **1996**, *47*, 247.

(19) Swiatla-Wojcik, D.; Buxton, G. V. *J. Phys. Chem.* **1995**, *99*, 11464.

(20) Bader, G.; Perluzzo, G.; Caron, L. G.; Sanche, L. *Phys. Rev. B* **1982**, *26*, 6019.

(21) Michaud, M.; Sanche L. *Phys. Rev. A* **1987**, *36*, 4684.

(22) Hochanadel, C. J.; Ghormley, J. A. *Radiat. Res.* **1962**, *16*, 653.

(23) Pimblott, S. M.; LaVerne, J. A. *Radiat. Res.* **1998**, *150*, 159.

(24) Green, N. J. B.; Pilling, M. J.; Pimblott, S. M.; Clifford, P. *J. Phys. Chem.* **1990**, *94*, 251. Pimblott, S. M.; Pilling, M. J.; Green, N. J. B. *Radiat. Phys. Chem.* **1991**, *37*, 377.

(25) Goulet, T.; Fraser, M.-J.; Frongillo, Y.; Jay-Gerin, J.-P. *Radiat. Phys. Chem.* **1998**, *51*, 85.

(26) LaVerne, J. A.; Pimblott, S. M. *J. Phys. Chem.* **1993**, *97*, 3291.

(27) Elliot, A. J. *Rate Constants and g-Values for the Simulation of the Radiolysis of Light Water over the Range 0–300 °C*; Report AECL-11073; 1994. See also Elliot, A. J.; Ouellette, D. C.; Stuart, C. R. *The Temperature Dependence of the Rate Constants and Yields for the Simulation of the Radiolysis of Heavy Water*; Report AECL-11658; 1996.

(28) Elliot, A. J.; McCracken, D. R.; Buxton, G. V.; Wood, N. D. *J. Chem. Soc., Faraday Trans.* **1990**, *86*, 1539.

(29) Onsager, L. *Phys. Rev.* **1938**, *54*, 554.

(30) Akerlof, G. C.; Oshry, H. I. *J. Am. Chem. Soc.* **1950**, *72*, 2844. Kaatze, U. *J. Chem. Eng. Data* **1989**, *34*, 371. Archer, D. G.; Wang, P. *J. Phys. Chem. Ref. Data* **1990**, *19*, 371.

(31) Noyes, R. M. In *Progress in Reaction Kinetics*; Porter, G., Stevens, B., Eds.; Pergamon Press: Oxford, 1961; Vol. 1, p 129.

(32) Smoluchowski, M. v. *Z. Phys. Chem.* **1917**, *92*, 129.

(33) Debye, P. *Trans. Electrochem. Soc.* **1942**, *82*, 265.

(34) Goulet, T.; Jay-Gerin, J.-P. *J. Chem. Phys.* **1992**, *96*, 5076.

(35) Elliot, A. J.; Chenier, M. P.; Ouellette, D. C. *J. Chem. Soc., Faraday Trans.* **1993**, *89*, 1193.

(36) Kent, M. C.; Sims, H. E. *Proceedings of the 6th International Conference on Water Chemistry of Nuclear Reactor Systems*; British Nuclear Energy Society: London, 1992; p 153.

(37) Sunaryo, G. R.; Katsumura, Y.; Hiroishi, D.; Ishigure, K. *Radiat. Phys. Chem.* **1995**, *45*, 131. Ishigure, K.; Katsumura, Y.; Sunaryo, G. R.; Hiroishi, D. *Radiat. Phys. Chem.* **1995**, *46*, 557. Katsumura, Y.; Sunaryo, G.; Hiroishi, D.; Ishigure, K. *Prog. Nucl. Energy* **1998**, *32*, 113.

(38) These units for *g*-values (yields) are used throughout in this paper. For conversion into SI units: 1 part./100 eV $\approx$ 0.10364 μmol/J.

(39) Under those conditions, these reactions occur less as the temperature is increased.

(40) Buxton, G. V.; Stuart, C. R. *J. Chem. Soc., Faraday Trans.* **1995**, *91*, 279.

(41) Elliot, A. J.; Ouellette, D. C. *J. Chem. Soc., Faraday Trans.* **1994**, *90*, 837.

(42) Elliot, A. J.; Chenier, M. P.; Ouellette, D. C.; Koslowsky, V. T. *J. Phys. Chem.* **1996**, *100*, 9014.

(43) Swiatla-Wojcik, D.; Buxton, G. V. *J. Chem. Soc., Faraday Trans.* **1998**, *94*, 2135.

(44) $O(^1D)$ denotes here atomic oxygen in its singlet ^1D state.

(45) Schmidt, K. H.; Bartels, D. M. *Chem. Phys.* **1995**, *190*, 145.

(46) Christensen, H.; Sehested, K. *J. Phys. Chem.* **1986**, *90*, 186.

(47) Shiraishi, H.; Sunaryo, G. R.; Ishigure, K. *J. Phys. Chem.* **1994**, *98*, 5164.

(48) We should mention that the pH of pure water decreases with increasing temperature (see, for example, ref 1), reaching a minimum value of ~5.7 around 240 °C. In this range, the primary yields for gamma irradiation vary very little with pH (see refs 8 and 9). Those pH effects are taken into account in our simulations.

(49) Buxton, G. V.; Mackenzie, S. R. *J. Chem. Soc., Faraday Trans.* **1992**, *88*, 2833.

(50) Burns, W. G.; Marsh, W. R. *J. Chem. Soc., Faraday Trans. 1* **1981**, *77*, 197.

(51) For a compilation of experimental data, published through 1994, on the time-dependent yields of hydrated electrons in the low-LET radiolysis of pure liquid water, see Cobut, V.; Frongillo, Y.; Jay-Gerin, J.-P.; Patau, J. P. *J. Chim. Phys.* **1994**, *91*, 1018.

(52) Sumiyoshi, T.; Katayama, M. *Chem. Lett.* **1982**, 1887. Sumiyoshi, T.; Tsugaru, K.; Yamada, T.; Katayama, M. *Bull. Chem. Soc. Jpn.* **1985**, *58*, 3073.

(53) Jonah, C. D.; Matheson, M. S.; Miller, J. R.; Hart, E. J. *J. Phys. Chem.* **1976**, *80*, 1267. Pimblott, S. M.; LaVerne, J. A.; Bartels, D. M.; Jonah, C. D. *J. Phys. Chem.* **1996**, *100*, 9412.

(54) Let us recall that, for each subexcitation electron energy, there exists a specific distribution of electron thermalization distances. Our calculated distribution of r_{th} values at 25 °C, averaged over the ensemble of subexcitation electrons, is characterized by the most probable value of r_{th} equal to ∼25 Å, and by the average thermalization distance $\bar{r}_{th} = 92$ Å. This relatively large average r_{th} value comes from the presence of a long tail in the distribution, which indicates that a number of electrons travel large distances (up to ∼400 Å) from subexcitation to thermal energies (see refs 10 and 17).